Geophysical Research Letters

RESEARCH LETTER
10.1029/2023GL107701

Lagged Response of MJO Convection and Precipitation to Solar Ultraviolet Variations on Intraseasonal Time Scales

C. A. Hoopes[1,2], L. L. Hood[2], and T. J. Galarneau Jr.[3]

[1]Department of Hydrology and Atmospheric Sciences, The University of Arizona, Tucson, AZ, USA, [2]Lunar and Planetary Laboratory, The University of Arizona, Tucson, AZ, USA, [3]NOAA/OAR/National Severe Storms Laboratory, Norman, OK, USA

Key Points:

- Evidence of lagged responses of tropical convection and precipitation to short-term solar UV variations is found over six solar cycles
- The responses are due to solar effects on eastward propagation of the Madden-Julian oscillation across the Maritime Continent barrier
- Average precipitation rate differences following solar peaks and minima can be more than 20% of mean daily rates

Supporting Information:

Supporting Information may be found in the online version of this article.

Correspondence to:

C. A. Hoopes,
cahoopes@arizona.edu

Citation:

Hoopes, C. A., Hood, L. L., & Galarneau, T. J., Jr. (2024). Lagged response of MJO convection and precipitation to solar ultraviolet variations on intraseasonal time scales. *Geophysical Research Letters*, *51*, e2023GL107701. https://doi.org/10.1029/2023GL107701

Received 5 DEC 2023
Accepted 24 APR 2024

Author Contributions:

Conceptualization: C. A. Hoopes, L. L. Hood, T. J. Galarneau Jr.
Data curation: C. A. Hoopes, T. J. Galarneau Jr.
Formal analysis: C. A. Hoopes
Funding acquisition: L. L. Hood
Investigation: C. A. Hoopes
Methodology: C. A. Hoopes, L. L. Hood, T. J. Galarneau Jr.
Project administration: L. L. Hood
Resources: C. A. Hoopes, L. L. Hood, T. J. Galarneau Jr.
Software: C. A. Hoopes
Supervision: L. L. Hood
Validation: C. A. Hoopes, T. J. Galarneau Jr.
Visualization: C. A. Hoopes

Abstract Composite analyses of NOAA satellite-based outgoing longwave radiation data and ERA5 reanalysis data for nearly six solar maximum periods support the existence of a response of tropical convection and precipitation to short-term (~27-day) solar ultraviolet variations. Following solar UV peaks, the response consists of an increase in average convection and precipitation in the equatorial Indian Ocean and a decrease in the western and central tropical Pacific, with maximum amplitude at a lag of 4 to 8 days. The opposite occurs following short-term solar UV minima. The observed responses are most detectable when the Madden-Julian oscillation (MJO) is active and appear to be related to a reduced ability of the MJO to propagate across the Maritime Continent barrier following solar UV peaks relative to UV minima. A similar behavior has previously been found when the stratospheric quasi-biennial oscillation is in its westerly phase relative to its easterly phase.

Plain Language Summary Under solar maximum conditions, active regions on the sun produce strong variations of solar ultraviolet radiation on the solar rotational time scale (~27 days). We have analyzed data from NOAA satellites and ERA5 reanalysis for almost six solar maximum periods. The results indicate that these short-term solar ultraviolet variations affect tropical convection and precipitation. Following a peak in solar UV radiation, there is an increase in convection and precipitation in the equatorial Indian Ocean, and a decrease in the western and central tropical Pacific, with the most significant changes occurring 4 to 8 days later. The opposite happens after solar UV minima. These effects are most noticeable when the Madden-Julian Oscillation is active and seem linked to its inability to move across the Maritime Continent barrier after solar peaks compared to solar minima. Similar patterns have been observed with the stratospheric quasi-biennial oscillation in its westerly phase versus its easterly phase.

1. Introduction

The Madden-Julian Oscillation (MJO) is an eastward-propagating, convectively-coupled wave which functions as a key driver of sub-seasonal to seasonal convection and precipitation variability in the tropics (e.g., Jiang et al., 2020; Madden & Julian, 1994). The MJO generates a Rossby wave train that strongly influences weather in the extratropics on subseasonal time scales (e.g., Jiang et al., 2020; Zhang, C., 2013), and evolves continuously through eight phases. Each phase is associated with either suppressed or enhanced convection within sub-regions of the tropics that progress eastward with time. The MJO is initiated via interactions of convective events with global circumnavigating flow patterns (Zhang, F. et al., 2017) and is sometimes weakened over the Maritime Continent (MC) or even fails to propagate past it (Kim et al., 2014; Zhang, C. & Ling, 2017). This is known as the Maritime Continent "barrier" effect on MJO propagation.

Previous research has shown that the stratospheric quasi-biennial oscillation (QBO; Baldwin et al., 2001) modulates the strength of the MJO during boreal winter (Yoo & Son, 2016; Nishimoto & Yoden, 2017; for a review, see Martin et al., 2021). The modulation is such that the MJO is about 40% stronger and persists about 10 days longer during the easterly QBO phase (QBOE) than during the westerly phase (QBOW). As argued by Zhang, C. and Zhang, B. (2018), the QBO-MJO connection can be understood as an increased number of strong MJO days during QBOE in boreal winter due to a weaker MC barrier effect on MJO eastward propagation. It was found (their Figure 3) that composites of precipitation anomalies for tracked MJO events showed increased precipitation east of the MC barrier (located at about 100°E) during QBOE relative to QBOW, while reduced precipitation was found west of the barrier.

Writing – original draft: C. A. Hoopes, L. L. Hood
Writing – review & editing: C. A. Hoopes, L. L. Hood, T. J. Galarneau Jr.

While the physical mechanisms for the QBO-MJO connection are not fully understood, it is likely that QBO-related changes in static stability and vertical zonal wind shear in the tropical tropopause region are responsible for initiating the series of processes that produce a net strengthening of the MJO in QBOE relative to QBOW (e.g., Hood et al., 2023; Jiang et al., 2020; Yoo & Son, 2016). Positive feedbacks from below including cloud-radiative feedbacks (Sakaeda et al., 2020; Son et al., 2017) and QBO influences on the MJO-induced cold cap anomaly ahead of MJO convection (Hendon & Abhik, 2018; Kodera et al., 2023; Lim & Son, 2020) are likely necessary to explain the full amplitude of the observed modulation. Several studies have found that the QBO-MJO connection has strengthened significantly since the early 1980s, coinciding with long-term decreases in tropical static stability (Hood & Hoopes, 2023; Klotzbach et al., 2019; Sakaeda et al., 2020).

An early study by Takahashi et al. (2010) performed a simple frequency analysis for cloud amount using 25 years of OLR data and found that a ∼27-day variation is prominent during solar maximum years in the Western Pacific warm pool region. Later studies found a lagged tropospheric temperature response in the tropics to short-term (mainly ∼27-day) solar ultraviolet (UV) peaks and minima occurring under solar maximum conditions (Hood, 2016) as well as a lagged increase in the occurrence rate of strong MJO days following 27-day solar UV minima (Hood, 2018). The most consistent correlations of tropical tropospheric temperature deviations with solar variability were found when solar UV flux was assumed to be the solar forcing variable (Figure S5 of Hood, 2016). Following solar UV peaks, the hypothesized mechanism involves direct solar UV increases of ozone production and radiative heating in the upper stratosphere, a slowing of the residual meridional (Brewer-Dobson) circulation, relative downwelling in the tropics, and an increase in static stability in the tropical lower stratosphere (see, e.g., Figure 1 of Hood, 2018).

Eastward propagation of MJO convection, as determined by the MJO's phase, may also be affected by solar-induced changes in tropical lower stratospheric static stability. Hood (2016) found relatively few occurrences of MJO phases 1, 7, and 8, associated with MJO activity in the Pacific, at lags of up to 7 days following solar peaks. Hoffmann and von Savigny (2019) found an increased rate of MJO phases 2, 3, 6, and 7 at the time of short-term solar peaks, with a proportional reduction in occurrence for phases 1, 4, 5, and 8. This relationship was found to be especially strong when combined with an easterly phase of the QBO. These results suggest that the MJO may be less able to propagate past the MC barrier into the Pacific following short-term solar peaks, as also appears to be the case in the westerly QBO phase.

In this current work, the possible existence of lagged responses of tropical convection and precipitation to short-term solar UV variations is investigated. The extent to which these responses are related to inhibition or enhancement of eastward MJO propagation past the MC is also evaluated. Excluding the ongoing maximum, nearly six solar cycle maximum periods are available for analysis, allowing tests of the reproducibility of the results.

2. Data and Methods

To objectively characterize the intensity of tropical convection, daily outgoing longwave radiation (OLR) data were used. From 1974 to 2021, satellite-based OLR data originally compiled by Liebmann and Smith (1996) were obtained from NOAA's Physical Sciences Laboratory (PSL) on a 2.5° × 2.5° latitude/longitude grid. For the pre-satellite (1959–1973) period, 6-hourly OLR data were obtained from the ERA5 reanalysis (Bell et al., 2021; Hersbach et al., 2020). To characterize tropical precipitation, hourly ERA5 precipitation data on a 1° × 1° grid were downloaded for the 1959–2021 time period. These data were averaged onto a 3° × 3° grid and daily means were calculated. In addition, satellite-based precipitation data starting in July of 2000 from the Tropical Rainfall Measurement Mission (TRMM) and the Global Precipitation Measurement (GPM) mission were employed (Huffman et al., 2023).

To determine whether the MJO was active on a given day, the amplitude and principal components of the OLR-based MJO index (OMI; Kiladis et al., 2014) were obtained from NOAA for the period from 1979 to 2021. The OMI is a projection of 20–96-day filtered NOAA PSL OLR data onto the 1979–2012 EOFs of 30–96-day eastward-only filtered NOAA PSL OLR. OMI amplitudes are expressed in standard deviations. The MJO is considered as active for OMI > 1.0 standard deviations (s.d.). In addition, the Real-time Multivariate MJO (RMM) index (Wheeler & Hendon, 2004) was obtained from the Australian Bureau of Meteorology. As discussed by Yoo and Son (2016), it has been shown that the OMI correlates well with the RMM but better tracks the convective component of the MJO (Kiladis et al., 2014), which is of most interest for the present study.

Although the official OMI record only extends back to 1979, a reconstruction of the index back to 1974 using the NOAA PSL OLR data and the 1979–2012 EOFs was performed using the "mjoindices" Python package developed by Hoffmann et al. (2021). For the pre-satellite (1959–1973) period, the same package was applied to the ERA5 OLR data (see, e.g., Hood & Hoopes, 2023; their Section 2).

To determine the phase of the QBO, the radiosonde-measured equatorial 50 hPa zonal wind monthly means (u50) compiled at the Free University of Berlin (e.g., Naujokat, 1986) are employed.

To characterize solar UV variability, daily solar fluxes at 205 nm (F205) from version 2 of the Naval Research Laboratory solar spectral irradiance model (NRLSSI2) (Coddington et al., 2015; Lean, 2000) were used. The data were downloaded for the full analysis period from the Laboratory for Atmospheric and Space Physics at the University of Colorado. The 205 nm wavelength was chosen due to its location in the range of wavelengths that directly affect ozone production and radiative heating in the upper stratosphere, while still retaining large temporal variability by remaining short of the Al I edge (e.g., Hood, 2018). A plot of the daily F205 index is shown in Figure S1 in Supporting Information S1 for six solar cycles.

To isolate variability associated with short-term (27-day) solar fluctuations and maintain consistency with previous studies, the daily F205 flux data were filtered by calculating deviations of 5-day running means from 35-day running means (Figure S1b in Supporting Information S1). Daily time series of both the satellite OLR data and the ERA5 precipitation data at a given grid point were filtered in the same manner as was done for F205.

Figure S2 shows the filtered F205 flux data during 5-year intervals centered approximately on the maxima of the six solar cycles plotted in Figure S1 in Supporting Information S1. Time periods when the filtered flux variations were larger than average for a given cycle are indicated by brackets (excluding times prior to 1959 when the analyzed ERA5 data begin). For the post-1974 part of the record, these periods are the same as those considered in Hood (2016, 2018). All analyses of filtered OLR and precipitation daily time series were limited to these high-variability periods. To further improve the detectability of lagged responses, only relatively large (magnitude >0.1 mW m^{-2} nm^{-1}) filtered F205 peaks and minima within the bracketed periods were considered, as was done previously. A total of 137 qualifying peaks and 128 qualifying minima in cycles 21 to 24 were identified by this procedure within the bracketed intervals of Figure S2 in Supporting Information S1. Extension of the record back to 1959 yields an additional 38 peaks and 34 minima in cycles 19 and 20.

Precipitation and OLR data were composited at individual grid points for qualifying filtered peaks and minima at 2-day intervals, covering a complete 27-day cycle (-14 to $+14$ days). For both the OLR and precipitation data, the composited values were tested for significance at 95% confidence using a Monte Carlo (bootstrap) resampling method with replacement. Keeping the filtered OLR and precipitation data unchanged, the analysis is repeated 500 times with the times of the UV peaks and minima shifted at random (keeping relatively constant intervals between peaks and minima). If the magnitude of the composited value at a given grid point obtained in the original analysis is equaled or exceeded in less than 5% of the randomized composites, the value is considered as significant at 95% confidence. The 5-day averaging of the data had little or no effect on the significance testing since all UV peaks or minima were separated by at least 20 days.

3. Lagged Composite Analyses Relative to Solar UV Peaks and Minima

To ensure the best accuracy of the OLR and precipitation composites, analyses were initially limited to the 1979–2016 period when satellite OLR data were available under solar maximum conditions. Figures 1 and 2 show averages of composite analyses for this period of NOAA PSL OLR and ERA5 precipitation, respectively, at lags of +4, +6, and +8 days relative to strong solar UV peaks and minima during 1974–2021, selected as described in Section 2. Negative OLR anomalies, indicating higher cloud tops and therefore increased convection, are colored red. Positive precipitation anomalies are also colored red to be consistent with increased convection. Dots are plotted at all grid points (2.5° intervals for OLR and 3.0° intervals for precipitation) where composites were significant at 95% confidence. As a check on the accuracy of the ERA5 precipitation data, separate composite analyses were performed using TRMM/GPM satellite precipitation data, which are available from July 2000 onward. While not identical (Figures S3 to S6 in Supporting Information S1), the general pattern of the composited results is consistent using both data sets in that composited anomalies are mostly positive west of the MC and are mostly negative east of the MC. This supports the use of ERA5 data to extend the precipitation analysis to times prior to 2000.

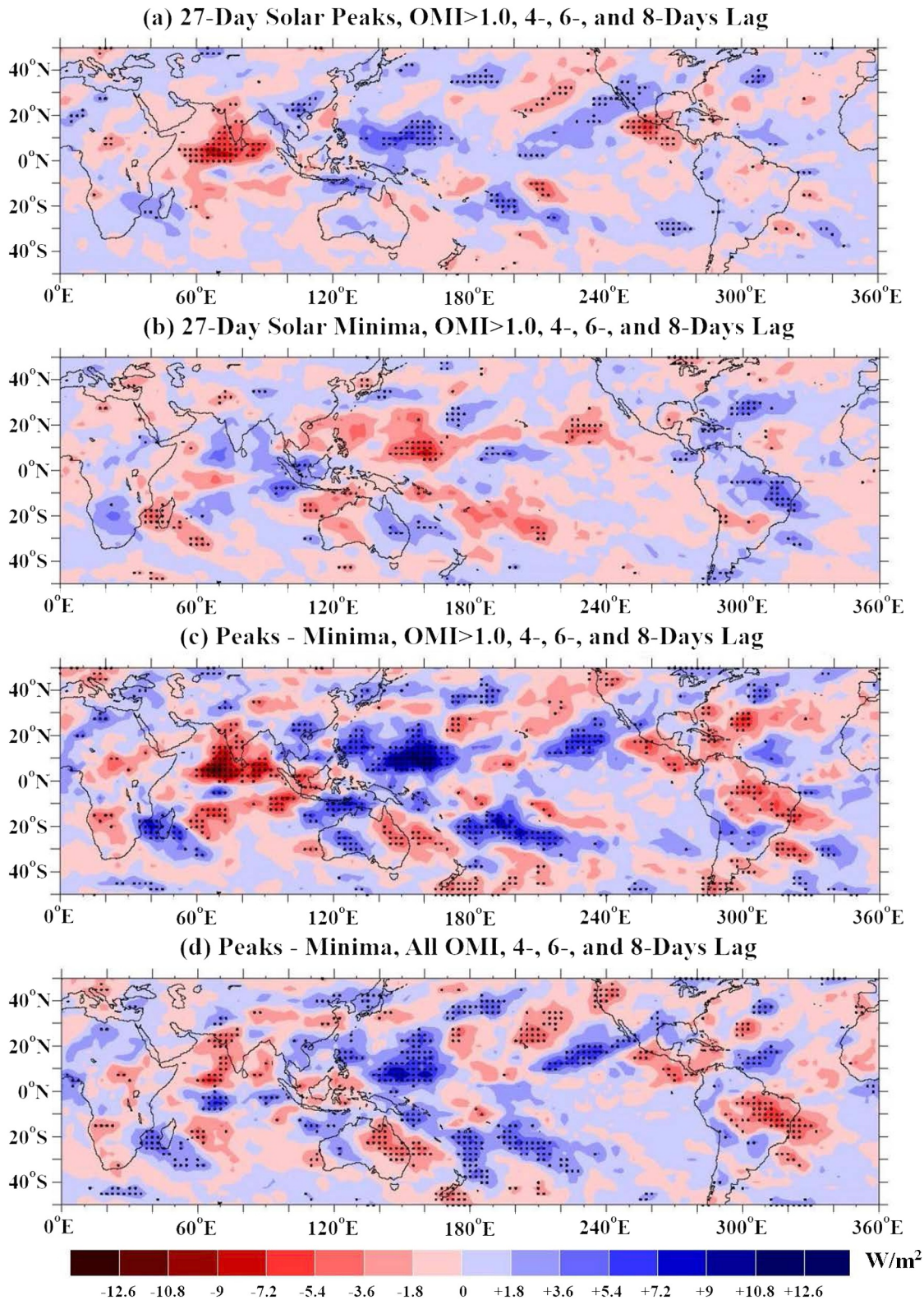

Figure 1. Composited means of 5 to 35-day filtered NOAA daily OLR anomalies for the 1979 to 2016 period. Shown in panels (a) and (b) are composites at combined lags of 4, 6, and 8 days following UV peaks and minima, respectively, considering only days with OMI > 1 s.d. Differences between (a) and (b) are shown in (c). Panel (d) shows differences considering all days with OMI > 0.

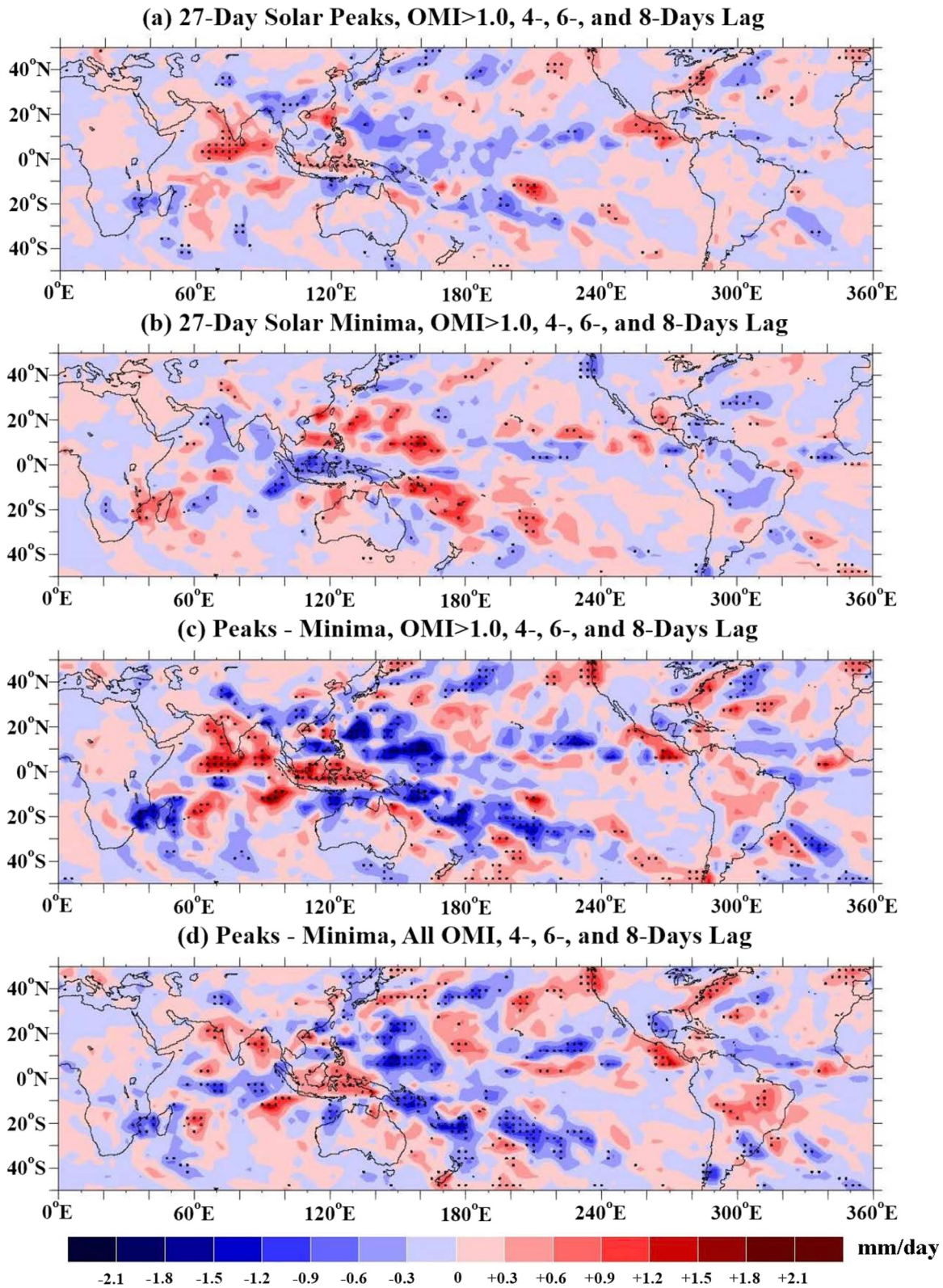

Figure 2. As in Figure 1 but for composited means of 5 to 35-day filtered ERA5 precipitation anomalies.

Figures 1a and 2a show composites relative to UV *peaks* for lagged days when the MJO was active (OMI >1 s.d.). This requirement reduced the number of available qualifying UV peaks from 137 to about 80–85, depending slightly on the lag. As seen in Figure 1a, a large positive (red) convection anomaly is present in the Indian Ocean, north of the equator, while relatively strong negative (blue) anomalies are present in the western and central Pacific. The MC region lies between the two. As seen in Figure 2a, a similar pattern of positive precipitation anomalies is present in the Indian Ocean while negative precipitation anomalies dominate in the western and central Pacific. Composite analyses of OLR and precipitation relative to UV peaks at individual lags of −10 to +12 days at 2-day intervals, representing most of a 27-day period, are shown in Figures S7 and S8 in Supporting Information S1. There it is seen that the OLR and precipitation anomalies evolve continuously from dominantly negative at negative lags to positive at positive lags in the Indian Ocean region and vice versa in the western and central Pacific.

Figures 1b and 2b show composites relative to UV *minima* for lagged days when the MJO was active (OMI > 1 s.d.). About 75 of the original 128 strong minima qualified as occurring when the MJO was active. Generally opposite patterns of OLR and precipitation anomalies in the Indian Ocean and western/central Pacific regions are found in comparison to those obtained following UV peaks. Composite analyses of OLR and precipitation relative to UV minima at individual lags are shown in Figures S9 and S10 in Supporting Information S1. The OLR and precipitation anomalies evolve continuously from dominantly positive at negative lags to negative at positive lags in the Indian Ocean region and vice versa in the western and central Pacific.

Figures 1c and 2c show the differences between the (a) and (b) panels. The same OLR and precipitation anomaly patterns seen in Figures 1a and 2a (composites relative to UV peaks) are generally found again but are larger in amplitude because of the combined responses to peaks and minima. Figures S11 and S12 in Supporting Information S1 show differences of the OLR and precipitation anomalies for OMI > 1 s.d. at individual lags. The same evolution with increasing lag of the OLR and precipitation anomalies as was found for composites relative to UV peaks is obtained, although with increased amplitude.

Figures 1d and 2d show differences between composites similar to those of the (a) and (b) panels but for all strong peaks (137) and minima (128) without restriction on MJO activity (i.e., for OMI > 0 s.d.). In the longitude range where the MJO is most active (60°E to 180°E), the amplitudes and statistical significance of the differenced composites in the (d) parts are noticeably reduced compared to those in the (c) parts for OMI > 1 s.d. Similar composite analyses for OMI > 0 s.d. at individual lags are shown in Figures S13 and S14 in Supporting Information S1. Although an evolution with increasing lag that is similar to that obtained in Figures S11 and S12 in Supporting Information S1 is found, at longitudes from 60°E to 180°E, composites are generally less statistically significant with weaker amplitudes. Repeating the differenced composites for OMI > 0.5 s.d. yields intermediate results (Figures S15 and S16 in Supporting Information S1). Overall, this implies a significant role of the MJO in producing the observed responses and their geographic distribution. Specifically, the stronger positive convection and precipitation anomalies in the Indian Ocean and negative anomalies in the western Pacific in Figures 1c and 2c when the MJO is active suggest that eastward propagation of the MJO past the MC barrier is inhibited following solar UV peaks relative to solar UV minima. We note that using the RMM index (RMM > 1 s.d.) to determine whether a UV peak or minimum occurred when the MJO was active yields similar results but with reduced anomaly amplitudes (Figures S17 and S18 in Supporting Information S1).

While many areas in Figures 1 and 2 are formally significant at 95% confidence, as much as 5% of the map areas can be significant by chance alone. As a check on the validity of the results, it is therefore useful to apply an alternate empirical test by determining the reproducibility of Figures 1 and 2 in different time periods. For this purpose, analyses at lags of 4, 6, and 8 days were repeated for three separate intervals: 1959–1971; 1979–1993; and 1999–2016 (Figure S1b in Supporting Information S1). The first period beginning in 1959 starts in the middle of the cycle 19 maximum and therefore covers about 1.5 maxima. The number of useable peaks or minima is reduced to around 25 for the pre-1973 period, around 35 for solar cycles 21 and 22 (1979–1993) and about 40 for solar cycles 23 and 24 (1999–2016). Results for OLR and precipitation are shown respectively in Figures S19 and S20 in Supporting Information S1 for 1959–1971, in Figures S21 and S22 in Supporting Information S1 for 1979–1993, and in Figures S23 and S24 in Supporting Information S1 for 1999–2016. There it is seen on the difference maps in the 60°E to 180°E longitude range that fewer grid points are significant and amplitudes are reduced compared to those in Figures 1c and 2c, as expected from the reduced number of useable UV peaks and minima.

Comparing the OLR and precipitation composite results for the three separate time intervals to those for the 1979 to 2016 period shown in Figures 1 and 2, it is first seen that the basic patterns of stronger or weaker convection and precipitation west and east of the MC found in Figures 1a–1c and 2a–2c are also present in each of the three time intervals. This supports the reality and reproducibility of these basic patterns, at least for the strong solar UV peaks and minima considered here. At tropical latitudes, a number of individual regional areas also show at least partially consistent signals in the three time intervals. For example, anomaly differences in Figures 1c and 2c are positive in the Indian Ocean north of the equator and negative in the western Pacific north of the equator during the three intervals, although these signals are weaker during 1973–1993. Positive anomaly differences are obtained over northeastern Australia in the three time intervals, although again less so during 1973–1993. Outside of both the tropics and the 60°E to 180°E longitude range where the MJO is most active, little reproducibility of composited anomalies is obtained during any two of the three intervals. Any small regional anomalies in Figures 1 and 2 with formally significant grid points that do not at least partially repeat in two or more of the three time intervals are not confirmed as reliable in this study.

To investigate possible seasonal dependences of these results, OLR and precipitation anomaly composites for the 1979 to 2016 period were repeated considering only the Northern Hemisphere cool (November-April) and warm (May-October) seasons. Of the 81 selected UV peaks in that time period with OMI > 1 s.d., 41 occurred during the cool season and 40 occurred during the warm season. Of the 69 qualifying UV minima, 38 occurred during the cool season and 31 occurred during the warm season. As seen in Figure S25 in Supporting Information S1, positive and negative composited differences west and east of the MC are mainly present north of the equator during the warm season and south of the equator during the cool season. This is consistent with the seasonal shift of the intertropical convergence zone where most tropical convection, including MJO convection, tends to be centered on. The largest regions of strong anomaly differences are found north of the equator in the Indian Ocean and Western Pacific during the warm season. These seasonal differences reduced the full-year amplitudes shown in Figures 1 and 2.

Finally, for the same period, OLR and precipitation anomaly composites were repeated for times with OMI >1 s.d. when the QBO was in an easterly phase (u50 < 0; 38 peaks and 32 minima) and a westerly phase (u50 > 0; 43 peaks and 37 minima). As seen in Figures S26 and S27 in Supporting Information S1, the OLR anomaly differences between peaks and minima in the (c) parts appear to be somewhat stronger in QBOE, especially the negative anomalies west of the MC. Similarly, in Figures S28 and S29 in Supporting Information S1, precipitation anomaly differences in the (c) parts also appear to be somewhat stronger in QBOE than in QBOW, both east and west of the MC. These results may differ somewhat from those of Hoffmann and von Savigny (2019), who concluded that a solar 27-day influence on MJO phase evolution is only detectable under QBOE conditions.

4. MJO Phase Behavior Following UV Peaks and Minima

In this section, to investigate further the suggested interpretation of the previous section (i.e., that eastward propagation of MJO convection past the MC barrier is inhibited following peaks in solar UV flux and promoted following UV minima), the number of days in each of the eight OMI MJO phases is calculated at lags of +4, +6, and +8 days for qualifying strong UV peaks and minima in the post-1974 period. While the OMI MJO phase counts are based on the OLR data used above, they provide an alternate means of measuring the rate of MJO propagation past the MC barrier. They are independent of the precipitation data, which also suggest the same interpretation.

In Table 1, the first three pairs of columns list the total number of days when the MJO was in each phase at each of the three lags following strong UV peaks and minima. Only days with an active MJO (OMI > 1 s.d.) are counted. The last pair of columns lists the totals for all three lags combined. For MJO phases 1, 5, 7, and 8, the total number of days does not differ significantly between minima and peaks. However, for MJO phases 2, 3, 4, and 6, relatively large differences (i.e., differences greater than 50%) are obtained and the totals are shown in bold type. For phases 3 and 4, differences are more than a factor of two, which Monte Carlo simulations indicate can occur by chance less than 5% of the time. The relative increase in MJO phases 2, 3, and 4 following solar peaks implies that the MJO is spending more time in the Indian Ocean following such peaks, while the increase in Phase 6 following solar minima implies enhanced MJO propagation past the MC barrier and into the Pacific following such minima. The largest change from one phase to the next (8–31 days) occurs following UV minima in transitioning from MJO Phase 4 to 5. This latter result may be consistent with behavior previously reported by Hoffmann and von Savigny (2019). It reflects a relatively short time following UV minima spent by MJO convection in Phase 4 when convection maximizes over the MC, that is, a relatively fast traversal of the MC. Similar but opposite phase count

Table 1
MJO Phase Counts Relative to Solar UV Peaks and Minima (1979–2016)

	+4 Days		+6 Days		+8 Days		Total	
MJO phase	Minima days	Peak days	Minima days	Peak days	Minima days	Peak days	Minima days	Peak days
1	9	7	9	12	8	10	26	29
2	10	12	7	10	5	11	**22**	**33**
3	7	16	7	17	9	15	**23**	**48**
4	2	8	3	9	3	8	**8**	**25**
5	11	10	11	11	9	8	31	29
6	11	9	11	4	14	8	**36**	**21**
7	13	12	8	12	9	10	30	34
8	9	9	12	8	10	9	31	26

differences are obtained at negative lags relative to UV peaks and minima (not shown), representing responses to prior UV minima and peaks, respectively. Also consistent with results of Hoffmann and von Savigny (2019), use of the RMM index instead of OMI to count MJO phases yields much less definitive results with differences of more than 50% in Phase 3 but not in phases 2, 4, and 6 (Table S1 in Supporting Information S1). This is to be expected since, as mentioned in Section 2, the OMI better represents the convective component of the MJO, which is of most interest here.

5. Discussion

Overall, these results indicate that, on average, under solar maximum conditions, short-term increases in solar UV radiation inhibit the ability of the MJO to propagate eastward across the Maritime Continent barrier. The opposite happens following short-term solar UV minima. While the implemented approach is statistical, a possible physical mechanism exists as summarized in the Introduction. These results may be consistent with early spectral analyses of OLR data, which reported peaks in 25–29 days spectral power located west and east of the MC (Takahashi et al., 2010; see their Figure 1).

Amplitudes in the affected regions are not negligible. For example, the mean daily precipitation rate in Singapore is 6.4 mm/day while the mean difference in precipitation following solar UV peaks and minima at this location was more than 1.2 mm/day or about 19% (Figure 2c). The mean precipitation rate on the island of Guam is about 6.8 mm/day. According to Figure 2c, the mean difference in precipitation in the Guam region following solar UV peaks and minima is about −1.2 to −1.5 mm/day, or up to −22%.

In addition to effects on tropical weather, indirect effects on weather events at northern midlatitudes are possible due to the different lengths of time spent by MJO convection west or east of the MC following solar UV peaks and minima. Previous work (e.g., Guo et al., 2017; Lee & Lim, 2012) has found a poleward shift in the North Pacific storm track (NPST) following an active MJO in the Indian Ocean region (phases 2 and 3) and an equatorward storm track shift in the same region following high MJO convective activity over the Pacific (phases 6–8).

The current results apply specifically to the ∼27-day solar rotational time scale. However, observational evidence on this time scale supports the view that similar effects should also occur on the 11-year time scale. Thus, MJO eastward propagation across the MC barrier may also be inhibited near 11-year solar maxima relative to solar minima. In combination with the QBO influence, which is mainly observed during boreal winter, the 11-year solar influence should be such that MJO eastward propagation across the MC barrier is most favored under combined QBOE and solar minimum conditions (e.g., Hood, 2017).

Data Availability Statement

ERA5 reanalysis data (Bell et al., 2021; Hersbach et al., 2020) were obtained from the Copernicus Climate Data Store (https://cds.climate.copernicus.eu/cdsapp#!/home). The OLR-based MJO index (OMI) data (Kiladis et al., 2014) were obtained from www.esrl.noaa.gov/psd/mjo/mjoindex while the Real-time multivariate MJO

(RMM) index data (Wheeler & Hendon, 2004) were obtained from http://www.bom.gov.au/climate/mjo. OLR data were obtained from NOAA at https://psl.noaa.gov/data/gridded/data.olrcdr.interp.html. The TRMM/GPA precipitation data (Huffman et al., 2023) were obtained from https://disc.gsfc.nasa.gov/datasets/GPM_3IMERGDF_07/summary?keywords=%22IMERG%20final%22. Solar data at 205 nm (Coddington et al., 2015; Lean, 2000) were obtained from http://lasp.colorado.edu/lisird/data/nrl2_files. Equatorial zonal wind data for determining the phase of the QBO (Naujokat, 1986) were obtained from https://www.geo.fu-berlin.de/met/ag/strat/produkte/qbo/qbo.dat. OMI data for years prior to 1974 were calculated using ERA5 OLR data and the Python package produced by Hoffmann et al. (2021), available at http://dx.doi.org/10.5281/zenodo.3613752.

Acknowledgments
Support for this work came from the NASA Living with a Star program (80NSSC21K1309) and the NSF Climate and Large-Scale Dynamics program (2039384). We also thank both reviewers for their useful criticisms which were used to improve the manuscript.

References

Baldwin, M. P., Gray, L. J., Dunkerton, T. J., Hamilton, K., Haynes, P. H., Randel, W. J., et al. (2001). The quasi-biennial oscillation. *Reviews of Geophysics*, *39*(2), 179–229. https://doi.org/10.1029/1999RG000073

Bell, B., Hersbach, H., Simmons, S., Berrisford, P., Dahlgren, P., Horanyi, A., et al. (2021). The ERA5 global reanalysis: Preliminary extension to 1950. *Quarterly Journal of the Royal Meteorological Society*, *147*(741), 4186–4227. https://doi.org/10.1002/qj.4174

Coddington, O., Lean, J. L., Pilewskie, P., Snow, M., & Lindholm, D. (2015). A solar irradiance climate data record. *Bulletin of the American Meteorological Society*, *97*(7), 1265–1282. https://doi.org/10.1175/BAMS-D-14-00265.1

Guo, Y., Shinoda, T., Lin, J., & Chang, E. K. M. (2017). Variations of Northern Hemisphere storm track and extratropical cyclone activity associated with the Madden–Julian oscillation. *Journal of Climate*, *30*(13), 4799–4818. https://doi.org/10.1175/JCLI-D-16-0513.1

Hendon, H. H., & Abhik, S. (2018). Differences in vertical structure of the Madden-Julian Oscillation associated with the quasi-biennial oscillation. *Geophysical Research Letters*, *45*(9), 4419–4428. https://doi.org/10.1029/2018GL077207

Hersbach, H., Bell, B., Berrisford, P., Hirahara, S., Horanyi, A., Munoz-Sabater, J., et al. (2020). The ERA5 global reanalysis. *Quarterly Journal of the Royal Meteorological Society*, *146*(730), 1999–2049. https://doi.org/10.1002/qj.3803

Hoffmann, C. G., Kiladis, G. N., Gehne, M., & von Savigny, C. (2021). A Python package to calculate the OLR-based index of the Madden-Julian oscillation (OMI) in climate science and weather forecasting. *Journal of Open Research Software*, *9*, 1–11. https://doi.org/10.5334/jors.331

Hoffmann, C. G., & von Savigny, C. (2019). Indications for a potential synchronization between the phase evolution of the Madden-Julian oscillation and the solar 27-day cycle. *Atmospheric Chemistry and Physics*, *19*(7), 4235–4256. https://doi.org/10.5194/acp-19-4235-2019

Hood, L. L. (2016). Lagged response of tropical tropospheric temperature to solar ultraviolet variations on intraseasonal time scales. *Geophysical Research Letters*, *43*(8), 4066–4075. https://doi.org/10.1002/2016GL068855

Hood, L. L. (2017). QBO/solar modulation of the boreal winter Madden-Julian oscillation: A prediction for the coming solar minimum. *Geophysical Research Letters*, *44*(8), 3849–3857. https://doi.org/10.1002/2017GL072832

Hood, L. L. (2018). Short-term solar modulation of the Madden-Julian climate oscillation. *Journal of the Atmospheric Sciences*, *75*(3), 857–873. https://doi.org/10.1175/JAS-D-17-0265.1

Hood, L. L., & Hoopes, C. A. (2023). Arctic sea ice loss, long-term trends in extratropical wave forcing, and the observed strengthening of the QBO-MJO connection. *Journal of Geophysical Research*, *128*(24), e2023JD039501. https://doi.org/10.1029/2023JD039501

Hood, L. L., Trencham, N. E., & Galarneau, T. G. (2023). QBO/Solar influences on the tropical Madden-Julian Oscillation: A mechanism based on extratropical wave forcing in late fall and early winter. *Journal of Geophysical Research: Atmospheres*, *128*(6), e2022JD037824. https://doi.org/10.1029/2022JD037824

Huffman, G. J., Stocker, E. F., Bolvin, D. T., Nelkin, E. J., & Tan, J. (2023). GPM IMERG final precipitation L3 1 day 0.1 degree x 0.1 degree V07 [Dataset]. *Goddard Earth Sciences Data and Information Services Center*. https://doi.org/10.5067/GPM/IMERGDF/DAY/07

Jiang, X., Adames, A. F., Kim, D., Maloney, E. D., Lin, H., Kim, H., et al. (2020). Fifty years of research on the Madden-Julian oscillation: Recent progress, challenges, and perspectives. *Journal of Geophysical Research: Atmospheres*, *125*(17), 1–64. https://doi.org/10.1029/2019JD030911

Kiladis, G. N., Dias, J., Straub, K. H., Wheeler, M. C., Tulich, S. N., Kikuchi, K., et al. (2014). A comparison of OLR and circulation-based indices for tracking the MJO. *Monthly Weather Review*, *142*(5), 1697–1715. https://doi.org/10.1175/MWR-D-13-00301.1

Kim, D., Kug, J., & Sobel, A. H. (2014). Propagating versus non-propagating Madden-Julian oscillation events. *Journal of Climate*, *27*(1), 111–125. https://doi.org/10.1175/JCLI-D-13-00084.1

Klotzbach, P., Abhik, S., Hendon, H. H., Bell, M., Lucas, C., Marshall, A. G., & Oliver, E. C. J. (2019). On the emerging relationship between the stratospheric quasi-biennial oscillation and the Madden-Julian oscillation. *Scientific Reports*, *9*, 1–9. https://doi.org/10.1038/s41598-019-40034-6

Kodera, K., Nasuno, T., Son, S.-W., Eguchi, N., & Harada, Y. (2023). Influence of the stratospheric QBO on seasonal migration of the convective center across the Maritime Continent. *Journal of the Meteorological Society of Japan*, *101*(6), 445–459. https://doi.org/10.2151/jmsj.2023-026

Lean, J. (2000). Evolution of the sun's spectral irradiance since the Maunder Minimum. *Geophysical Research Letters*, *27*(16), 2425–2428. https://doi.org/10.1029/2000GL000043

Lee, Y., & Lim, G. (2012). Dependency of the North Pacific winter storm tracks on the zonal distribution of MJO convection. *Journal of Geophysical Research*, *27*(D14), 1–12. https://doi.org/10.1029/2011JD016417

Liebmann, B., & Smith, C. A. (1996). Description of a complete (interpolated) outgoing longwave radiation dataset. *Bulletin of the American Meteorological Society*, *77*, 1275–1277. https://doi.org/10.1175/1520-0477-77.6.1274

Lim, Y., & Son, S.-W. (2020). QBO wind influence on MJO-induced temperature anomalies in the upper troposphere and lower stratosphere in an idealized model. *Journal of the Atmospheric Sciences*, *79*(9), 2219–2228. https://doi.org/10.1175/JAS-D-21-0296.1

Madden, R. A., & Julian, P. R. (1994). Observations of the 40-50-day tropical oscillation – A review. *Monthly Weather Review*, *122*(5), 814–837. https://doi.org/10.1175/1520-0493(1994)122%3C0814:OOTDTO%3E2.0.CO;2

Martin, Z., Son, S.-W., Butler, A., Hendon, H., Kim, H., Sobel, A., et al. (2021). The influence of the Quasi-Biennial Oscillation on the Madden–Julian Oscillation. *Nature Reviews Earth & Environment*, *2*(7), 477–489. https://doi.org/10.1038/s43017-021-00173-9

Naujokat, B. (1986). An update of the observed quasi-biennial oscillation of the stratospheric winds over the tropics. *Journal of the Atmospheric Sciences*, *43*(17), 1873–1877. https://doi.org/10.1175/1520-0469(1986)043<1873:AUOTOQ>2.0.CO;2

Nishimoto, E., & Yoden, S. (2017). Influence of the stratospheric quasi-biennial oscillation on the Madden-Julian oscillation during Austral summer. *Journal of the Atmospheric Sciences*, *74*(4), 1105–1125. https://doi.org/10.1175/JAS-D-16-0205.1

Sakaeda, N., Dias, J., & Kiladis, G. N. (2020). The unique characteristics and potential mechanisms of the MJO-QBO relationship. *Journal of Geophysical Research: Atmospheres*, *125*(17), e2020JD033196. https://doi.org/10.1029/2020JD033196

Son, S., Lim, Y., Yoo, C., Hendon, H. H., & Kim, J. (2017). Stratospheric control of the Madden-Julian oscillation. *Journal of Climate*, *30*(6), 1909–1922. https://doi.org/10.1175/JCLI-D-16-0620.1

Takahashi, Y., Okazaki, Y., Sato, M., Miyahara, H., Sakanoi, K., Hong, P. K., & Hoshino, N. (2010). 27-day variation in cloud amount in the Western Pacific warm pool region and relationship to the solar cycle. *Atmospheric Chemistry and Physics*, *10*(4), 1577–1584. https://doi.org/10.5194/acp-10-1577-2010

Wheeler, M. C., & Hendon, H. H. (2004). An all-season real-time multivariate MJO Index: Development of an index for monitoring and prediction. *Monthly Weather Review*, *132*(8), 1917–1932. https://doi.org/10.1175/1520-0493(2004)132%3C1917:AARMMI%3E2.0.CO;2

Yoo, C., & Son, S. (2016). Modulation of the boreal wintertime Madden-Julian oscillation by the stratospheric quasi-biennial oscillation. *Geophysical Research Letters*, *43*(3), 1392–1398. https://doi.org/10.1002/2016GL067762

Zhang, C. (2013). Madden–Julian oscillation: Bridging weather and climate. *Bulletin of the American Meteorological Society*, *94*(12), 1849–1870. https://doi.org/10.1175/BAMS-D-12-00026.1

Zhang, C., & Ling, J. (2017). Barrier effect of the Indo-Pacific maritime Continent on the MJO: Perspectives from tracking MJO precipitation. *Journal of Climate*, *30*(9), 3439–3459. https://doi.org/10.1175/JCLI-D-16-0614.1

Zhang, C., & Zhang, B. (2018). QBO-MJO connection. *Journal of Geophysical Research: Atmospheres*, *123*(6), 2957–2967. https://doi.org/10.1002/2017JD028171

Zhang, F., Taraphdar, S., & Wang, S. (2017). The role of global circumnavigating mode in the MJO initiation and propagation. *Journal of Geophysical Research: Atmospheres*, *122*(11), 5837–5856. https://doi.org/10.1002/2016JD025665